Doppler Spectrum of a Rotating Smooth Cylinder

Thomas Pairon, Christophe Craeye, Claude Oestges
Institute of Information and Communications Technologies, Electronics and Applied Mathematics (ICTEAM)
Universite Catholique de Louvain, Louvain-la-Neuve, Belgium
Email : {thomas.pairon,christophe.craeye,claude.oestges}@uclouvain.be

***Abstract*—The Doppler spectrum of a rotating smooth cylinder is investigated both theoretically and experimentally. Since the studied object has a smooth surface and is large compared to the wavelength, the physical optics (PO) approximation is used. The integration of the surface currents is computed with a hybrid method which consists of integrating analytically the currents in one dimension using the stationary phase method (SPM), while the currents in the other dimension are integrated numerically. This enables a reduction of the computation time compared to a fully numerical integration. Simulations are compared with measurements.**

***Index Terms*—Doppler spectrum, physical optics, stationary phase method, hybrid integration.**

I. Introduction

In many Doppler radar applications, the spectral shape of the radar cross-section is of interest. For instance, in the meteorological domain, rain radar measurements are disturbed by the presence of wind turbines. Due to their size, those wind turbines have a high reflectivity which is varying over time (rotating blades and nacelle aligned with the wind direction). The movement of those different parts generates a Doppler spectrum that leads to a wrong estimation of the rainfall rate in regions just behind the wind farms [1].

In defense applications, the Doppler spectrum provides important information about the structure of the target, *e.g.* the number of blades for a helicopter, that could be used for target classification [2]. The discrimination between different types of moving targets is also needed in civilian applications, such as road monitoring, with the objective of determining which kind of vehicle is on the road.

The computation of the scattered field using the method of moments (MoM) is no longer suitable for problems with large electrical sizes (*e.g.* $2300\ \lambda$ for a 125 m wind turbine at a frequency of 5.6 GHz). A fast algorithm using the shooting and bouncing ray technique (SBR) was presented in [3]. The proposed algorithm takes advantage of the instantaneous Doppler information available for each ray being traced through the target. This enables a noticeable speed-up of the computations.

When the object is electrically large and smoothly-shaped, asymptotic methods lead to accurate estimations. A commonly used method is the physical optics (PO) approximation [4]. In [5], the PO is combined with the method of equivalent current (MEC). The Doppler spectrum is computed assuming the quasi-stationarity of the process. This is realistic when the relativistic effects can be neglected. The scattered field is computed for each angle, which leads to the Doppler spectrum of the object by taking the Fourier Transform (FT).

In [6], the authors propose a new fast technique to evaluate numerically the PO integral by adding different contributions, *i.e.* stationary phase points, end points, etc. The integration surface is divided in small triangles and the computational speed up is obtained by emptying the triangles having a negligible contribution to the total radiated field. This method leads to CPU computational time independent of frequency.

Some improvements of the stationary phase method (SPM) are found in the literature, such as [7]. This method proposes a frequency-independent integration scheme for surface scattering problems in three dimensions which is considered as an extension of the the SPM. It consists on a analytic-numerical algorithm which allow the integration of oscillatory functions and can handle the difficulty when singular points and stationary phase points are close.

When the studied object has sharp edges, one has to take diffracted fields into account. Recently, authors used a method based on PO approximation for the smooth parts and the physical theory of diffraction (PTD) for the edges [8].

In this paper, we study the Doppler spectrum using the backscattered electric field from a smooth object and consider a cylinder with hemispherical ends as an example. The hemispherical ends offer a smooth shape for the entire object, which has an electrical length of about $30\ \lambda$. The PO approximation is used to compute backscattered fields generated by the incident wave. Those fields are computed using a hybrid integration scheme : in the horizontal plane, the currents are integrated analytically using the SPM, based on the analytical expression of the surface shape. This approach avoids facetting the surface, which often complicates the calculations. In the vertical plane, the currents are integrated numerically.

The remainder of this paper is organized as follows. In the section II, we remind the PO solution over the surface. In section III, the hybrid integration scheme is presented. Summing up all the contributions corresponding to each sampled angle of rotation and taking the Fourier transform, one obtains the Doppler spectrum of the cylinder. Section IV describes the experimental setup used for validation. Simulations and measurements are compared and discussed. We conclude this paper with some comments and perspectives.

II. PO formulation

This section is divided into three parts. In subsection II-A, we present all the parameters of the problem and derive the

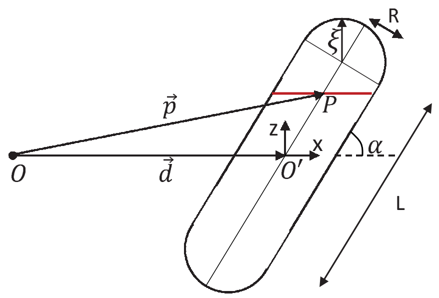

Fig. 1. Cylinder : xz-plane.

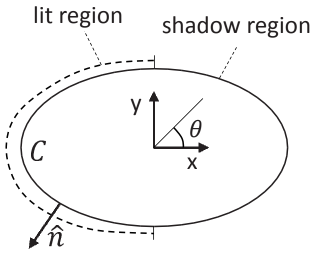

Fig. 2. Cylinder : xy-plane.

expression of the surface currents. Then the problem is divided in two parts : the cylindrical part of the object (subsection II-B) and the hemispherical ends (subsection II-C).

A. Description of the problem

The rotating cylinder is represented in Fig. 1. The object rotates around $(x, y, z) = (0, 0, 0)$ in the xz-plane. R is the radius of the cylinder, also equal to the radius of the hemispherical ends; L is the length of the cylindrical part of the object; α is the angle of inclination; O the source point and corresponds to the observation point in the mono-static case; O' is the origin of the cylinder, $|\vec{d}|$ represents the distance between the source point O and the origin of the cylinder O'; $|\vec{p}|$ represents the distance between the source point and the point P on the cylinder at a given L_i and $\hat{p}$ is the unitary vector from O to P.

For a given L_i, we take the horizontal slice passing through the considered point L_i. This slice is illustrated in Fig. 2. The parametric equation of the contour C of each slice is given by the following formula :

$$C(\theta) = \frac{R\cos\theta}{\sin\alpha}\hat{x} + R\sin\theta\hat{y} \tag{1}$$

The surface currents are expressed by the PO approximation as follow, *i.e* $\vec{J}_{\text{PO}}(\vec{r}) = 2\hat{n} \times \vec{H}^i$ in the lit region and $\vec{J}_{\text{PO}}(\vec{r}) = 0$ in the shadow region, with $\vec{H}^i$ is the incident magnetic field.

We suppose a TEM incident wave described by (we assume the factor $e^{j\omega t}$ for the sake of simplicity) :

$$\begin{aligned} \vec{E}^i &= E_0\,\hat{p} \times \hat{y} \\ \vec{H}^i &= -\frac{E_0}{\eta}\,\hat{y} \end{aligned} \tag{2}$$

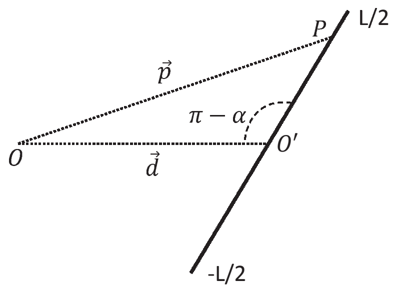

Fig. 3. Phase shift due to the inclination.

The outward normal $\hat{n}$ is expressed as :

$$\hat{n} = \sin\alpha\cos\theta\,\hat{x} + \sin\theta\,\hat{y} + \cos\alpha\cos\theta\,\hat{z} \tag{3}$$

Combining (1), (2) and (3), the surface current is given by

$$\vec{J}_{\text{PO}} = 2\frac{E_0}{\eta}\left(\cos\alpha\cos\theta\,\hat{x} - \sin\alpha\cos\theta\,\hat{z}\right) \tag{4}$$

The electric field at the observation point (that is equivalent that the source point for a mono-static case) is expressed as :

$$\vec{E}(\vec{p}) = -\frac{j\eta}{2\lambda}\iint_C \frac{e^{-jkP'}}{P'}\vec{J}_{\perp,\text{PO}}(\vec{p})\,\mathrm{d}C \tag{5}$$

where η in the free-space impedance ($\eta \approx 377\Omega$) and $\vec{J}_{\perp,}$ is the perpendicular component of the direction of observation, defined by $\vec{J}_\perp = \left(\vec{J} - \left(\vec{J}\cdot\hat{u}\right)\hat{u}\right)$ where $\hat{u}$ is the direction of the unit vector from a point on the cylinder surface to the observation point. P' corresponds to the phase shift and attenuation at the observation point. This term has two contributions :

- phase shift due to the inclination,
- phase shift due to the elliptical shape of each slice of the cylinder.

B. Cylindrical part of the object

The first phase shift effect depends on α. This case is illustrated in Fig. 3. The phase factor is equal to :

$$e^{-2jk\Delta d_\alpha} = e^{-2jk|\vec{p}-\vec{d}|} \tag{6}$$

with

$$\Delta d_\alpha = \sqrt{D^2 + l^2 + 2Dl\cos\alpha} - D \tag{7}$$

where $l \in [-L/2\,;\,L/2]$.

The second phase shift comes from the contour of each slice of the cylindrical part. In the case of a cylinder with a circular cross-section, the shape of each slice corresponds to an ellipse. The contour of the lit region, around the point of impact of the incident ray, is approximated by a parabola. With reference to Fig. 2, the contour of the lit region can be approximated by the following expression :

$$\Delta d_\theta \simeq \frac{1}{R\sin\alpha}\left(y^2 - R^2\right) \tag{8}$$

Inserting (7) and (8) into (5), the scattered field for each slice of the cylindrical part of the object is expressed as :

$$\mathrm{d}\vec{E}(\vec{r}) = -\frac{2}{D^2}\frac{j\eta}{2\lambda}\frac{E_0}{\eta}e^{-2jk\Delta_{d_\alpha}}[\cos\alpha\,\hat{x} - \sin\alpha\,\hat{z}] \int_{C'} \cos\theta\, e^{2jk\Delta_{d_\theta}}\,\mathrm{d}C'\,\mathrm{d}l \tag{9}$$

In polar coordinates, (9) can be written as :

$$\mathrm{d}\vec{E}(\vec{r}) = -\frac{j}{\lambda}\frac{1}{D^2}\frac{R}{\sin\alpha}E_0 e^{-2jk\Delta_{d_\alpha}}e^{-2jkR/\sin\alpha} [\cos\alpha\,\hat{x} - \sin\alpha\,\hat{z}] \int_{3\pi/2}^{\pi/2} I_{\text{ell}}(\theta)\,\mathrm{d}\theta\,\mathrm{d}l \tag{10}$$

with

$$I_{\text{ell}}(\theta) = \cos\theta\sqrt{\sin^2\theta + \sin^2\alpha\cos^2\theta}\; e^{2jkR\sin^2\theta/\sin\alpha} \tag{11}$$

C. Spherical part of the object

Analogous to section II-B, we can compute the phase shift due to the hemispherical ends of the object. In this case, the slices correspond to circles. There is a phase shift due to the position of the center of those slices and a second phase shift due to the circular contour.

In polar coordinates, the scattered electric field for each slice is expressed as follows :

$$\mathrm{d}\vec{E}(\vec{r}) = -\frac{j}{\lambda}\frac{1}{D^2}e^{-2jk\Delta_{d_\alpha}}R\sqrt{1-\xi^2}[\cos\alpha\,\hat{x} - \sin\alpha\,\hat{z}] \int_{3\pi/2}^{\pi/2} I_{\text{cir}}\,\mathrm{d}\theta\,\mathrm{d}l \tag{12}$$

with

$$I_{\text{circ}} = \begin{cases} \cos\theta\, e^{-2jkR\sqrt{1-\xi^2}\cos\theta} & \text{for}\, \xi\in[\cos\alpha\,;\,1] \\ \cos\theta\, e^{+2jkR\sqrt{1-\xi^2}\cos\theta} & \text{for}\, \xi\in[-1\,;\,\cos\alpha[\end{cases} \tag{13}$$

III. Integration scheme

As explained in the introduction, the integration scheme is based on a hybrid integration, *i.e.* an analytical integration for the contour of each slice and a numerical integration along l.

The current is integrated analytically on each slice using the SPM approximation. For the cylindrical part, the stationary phase point is located at $\theta = \pi$ for each slice of the cylinder. The value of the integral (10) is given by :

$$\mathrm{d}\vec{E}(\vec{r}) = \frac{j}{\lambda}\frac{1}{D^2}E_0 R\sqrt{\frac{\pi\sin\alpha}{2kR}}e^{-2jk\left(\frac{R}{\sin\alpha}-\frac{\pi}{8k}\right)}e^{-2jk\Delta_{d_\alpha}} [\cos\alpha\,\hat{x} - \sin\alpha\,\hat{z}] \tag{14}$$

For the hemispherical ends, (12) becomes :

$$\mathrm{d}\vec{E}(\vec{r}) = \frac{j}{\lambda}\frac{1}{D^2}E_0\sqrt{\frac{\pi R\sqrt{1-\xi^2}}{k}}e^{\mp 2jk\left(\Delta_{d_\alpha} - R\sqrt{1-\xi^2}+\frac{\pi}{8k}\right)} [\cos\alpha\,\hat{x} - \sin\alpha\,\hat{z}] \tag{15}$$

In (15), the $-$ case corresponds to the condition $\xi \in [\cos\alpha\,;\,1]$; the $+$ case corresponds to the condition $\xi \in [-1\,;\,\cos\alpha[$. The integral over the length L and the normalized radius ξ is computed numerically for each $\mathrm{d}\vec{E}(\vec{r})$ in (14) and (15) using a simple method.

IV. Results

This section is divided in two parts. The first one shows the results of the modelling obtained with the MATLAB® language. The second part shows the measurements of the scattered electric field captured with a radar, using a 3D-printed rotating cylinder with hemispherical ends covered with a conductive material. The object is fixed at its middle point on a DC motor. The measures are acquired using a RFBeam K-MC4 radar module which gives the quadrature components of the reflected electric field.

The parameters of the experimental setup used both for the simulations and measurements are the following :

- length of the cylinder : $L = 0.30$ m,
- radius of the cylinder : $R = 0.02$ m,
- frequency of the radar : $f_0 = 24.125$ GHz,
- distance from the source / to the observation point : $D = 1.5$ m,
- angular frequency : $\omega_r = 30.22$ rad/s.

A. Simulations

In order to obtain the Doppler spectrum of the rotating cylinder, we use the quasi-stationarity approximation. That means that we compute the scattered field by varying α and that, for each α, the cylinder is supposed at rest. Those computed values of the scattered field using (15) and (16) represent the time domain signal. The Doppler spectrum is obtained from a Fourier transform of the complex time-domain signal. The result is shown in Figs. 4 and 5 for time and frequency domains, respectively.

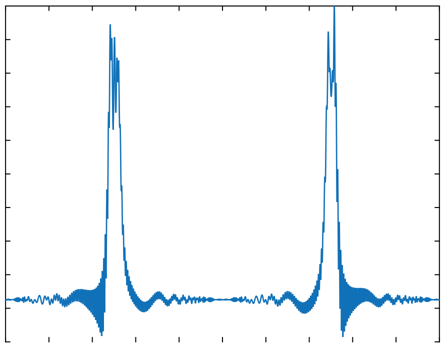

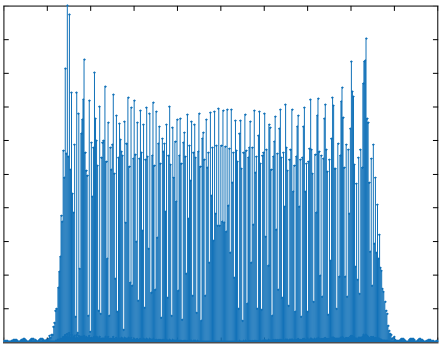

Fig. 5. Simulation of the rotating cylinder (frequency domain).

surface to increase the reflectivity of the cylinder. The results of the measurements are shown in Figs. 6 and 7.

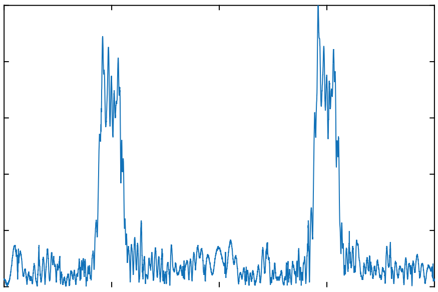

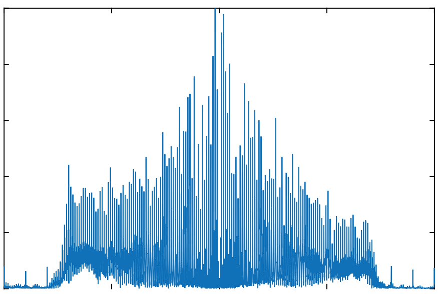

References

[1] Laurent Delobbe, IRM Brussels, oral communication, Aug 19th 2015.

[2] A. Cilliers and W.A.J. Nel, "Helicopter parameter extraction using joint time-frequency and tomographic techniques", *International Conference on Radar 2008*, pp.598-603, 2-5 Sept. 2008

[3] R. Bhalla and H. Ling, "A fast algorithm for simulation doppler spectra of targets with rotating parts using the shooting and boucing ray technique", *IEEE Trans. Antennas and Propagation*, vol.46, pp.1389-1391, Sep. 1998.

[4] R. F. Harrington, "Time-Harmonic Electromagnetic Fields", McGraw-Hill, p. 127, 1961.

[5] I. Tardy, G.-P. Piau, P. Chabrat and J. Rouch, "Computational and experimental analysis of the scattering by rotating Fans", *IEEE Trans. Antennas and Propagation*, vol.44, pp.1414-1421, Oct. 1996.

[6] F. Vico-Bondia and M. Ferrando-Bataller, "A new fast physical optics for smooth surfaces by means of a numerical theory of diffraction", *IEEE Trans. Antennas and Propagation*, vol. 58, March 2010.

[7] O. P. Bruno and C. A. Geuzaine, "An O(1) integration scheme for three-dimensional surface scattering problems", Journal of Computational and Applied Mathematics, 204, pp. 463-476, 2007.

[8] G. Jun and C. Xiangyu, "The Modulated Spectra Analysis of Backscattered Field Caused by Rotating Metal Airscrew", in *Chinese Journal of Electronics*, vol.17, no.4, Oct 2008.

[9] K-MC4 Monopulse Radar Transceiver, RFBeam Microwave GmbH, http://www.rfbeam.ch/fileadmin/downloads/datasheets/Datasheet_K-MC4.pdf